Photoacetylation of Diamondoids: Selectivities and Mechanism[‡]

Andrey A. Fokin,*[a,b] Pavel A. Gunchenko,[a] Anatoliy A. Novikovsky,[a]
Tatyana E. Shubina,[a] Boris V. Chernyaev,[a] Jeremy E. P. Dahl,[c] Robert M. K. Carlson,[c]
Alexander G. Yurchenko,[a] and Peter R. Schreiner*[b]

The photoacetylation of diamondoids (nanodiamonds), in particular [1212]pentamantane, [1(2,3)4]pentamantane, and [123]tetramantane, with diacetyl almost exclusively gives apical acetyl derivatives. The mechanism of the photoacetylation was studied on the basis of a comparative analysis of the experimental deuterium kinetic isotope effects as well as the observed C–H bond substitution selectivities, which were also computed at the B3LYP, B3PW91, and MP2 levels of theory including polarized continuum modeling of solvent effects. The high apical C–H bond selectivities in the photo-

acetylation of diamondoids are determined by the higher polarizabilities of the cages along the apical direction in the transition structures for hydrogen abstraction with the triplet diacetyl diradical. Steric effects play only a minor role, and in combination with solvation, outweigh charge-transfer effects that usually favor medial substitution with electrophiles and electrophilic radicals.

(© Wiley-VCH Verlag GmbH & Co. KGaA, 69451 Weinheim, Germany, 2009)

Introduction

Many promising applications were found recently for nanodiamond-based materials that display some unique properties, namely, hardness, chemical stability, high thermal conductivity, low density, and biocompatibility.[1–6] Nanometer-sized diamond (1.4–4.0 nm) is readily available from carbonaceous residues of detonations and from chemical vapor deposition (CVD)[7,8] but cannot be obtained as a homogeneous material with well-defined structures and particle dimensions;[9] further functionalization produces aggregated particles with broad size distributions and surface inhomogeneities.[10] In contrast, diamondoids, which are available from natural sources, represent 0.5–2 nm sized hydrogen-terminated nanodiamonds with distinct structures and particle shapes.[1,11,12] In contrast to other group IV nanoparticles they exhibit tunable electronic properties.[13,14] Among them, diamantane (**1**) and [121]tetramantane (**2**) are overall rod-shaped, triamantane (**3**) and [1212]pentamantane (**4**) have triangular shapes, [1(2)3]tetramantane (**5**) and [12312]hexamantane (cyclohexamantane, **6**)

display prismatic topologies, [1(2,3)4]pentamantane (**7**) is tetrahedral, and [123]tetramantane (**8**) shows helical topology (Figure 1).
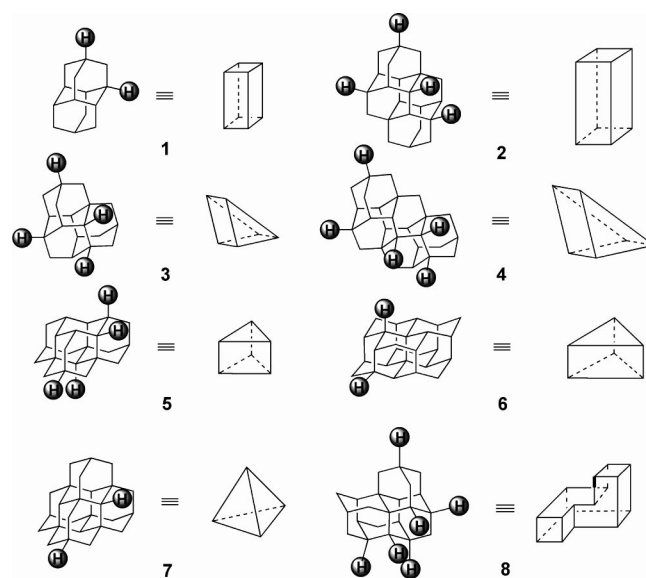

Figure 1. Diamondoids representing nanometer-sized particles with various topologies and increasing numbers of nonequivalent tertiary C–H bonds.

The large number of nonequivalent C–H bonds present in higher diamondoids makes their selective functionalizations rather difficult. Previously, we studied C–H substitution reactions in diamondoids in the presence of radical, electrophilic, and oxidative reagents[13,15–17] as part of our

---

mechanistic and preparative studies on alkane functionalizations.[18–24]

Differentiation between the secondary and tertiary C–H bonds can readily be achieved with strong electrophiles, which give tertiary derivatives exclusively. The true challenge is the selective substitution of certain types of tertiary C–H bonds. Increasing the diamondoid size and decreasing the symmetry of the cages usually leads to a large number of different tertiary C–H positions. For instance, whereas there are two different tertiary C–H bonds in highly symmetrical hydrocarbons 1, 6, and 7, there are four in less symmetrical 2, 3, and 5, five in structure 4, and even six in C_2-symmetrical 8 (Figure 1).

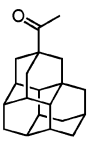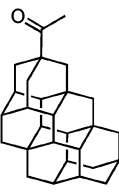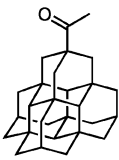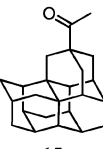The reactions of higher diamondoids with electrophiles often lead to mixtures of products whose distributions depend on the nature of the electrophilic reagent employed. Whereas brominations give predominantly mixtures of medial bromides,[15] nitroxylations usually lead to all possible tertiary nitroxy derivatives.[13,15,16,25] Generally, the medial diamondoid derivatives are less attractive for practical applications, because, due to steric hindrance, their surface binding energies are lower than that of the respective apical derivatives.[26] For instance, the apical thiolato derivative of 2 self-assembled on noble metal surfaces behaves as a highly efficient monochromatic photoelectron emitter.[27–29]

Previously, we developed a number of preparative methods for the apical functionalization of diamondoid derivatives.[15–17,25] The thermodynamically controlled transformations of diamondoids to diapical derivatives are quite selective but require multistep follow-up desymmetrization/reduction steps.[30] As we will demonstrate in the following, photooxidation with diacetyl is the only method that gives apical diamondoid derivatives directly. We also present mechanistic data that help rationalize this exceptional selectivity.

Results and Discussion

We have found previously that the photooxidations of higher diamondoids 2, 3, and 5 with diacetyl demonstrate unexpectedly high apical regioselectivities (Scheme 1).[13,15,16,25] For instance, although four different C–H bonds are present in 2 and 3 the respective apical derivatives 10 and 11 form with more than 80% selectivity and were obtained in high preparative yields from the photooxidation reaction.[16] We now studied the photoacetylation of other diamondoids depicted in Table 1 and found that the apical selectivity for acetylation of [1212]pentamantane (4, see Experimental Section for details) is even higher than that of parent 2 and 3[16] as well as that of diamantane (1).[31] Not even trace amounts of byproducts were found in the photoacetylation of [1(2,3)4]pentamantane (7). Although six different C–H bonds are present in 8 the apical derivative forms in 90% selectivity. Such C–H substitution selectivities are quite unusual in preparative alkane chemistry, and the origin of this effect is unclear.

Table 1. Selectivities for the photoacetylation of diamondoids with diacetyl (UV lamp, λ_{max} = 300 nm, CH$_2$Cl$_2$, r.t.) and preparative yields of the apical products.

Hydro-carbon	Product	Apical selectivity [%]	Yield [%]	Ref.
1	9	82	62	[13, 31]
2	10	82	57[a]	[16]
3	11	88	43[b]	[16]
4	12	85	51	this work
5	13	95	53	[25]
7	14	~100	45[c]	this work
8	15	90	58	this work

[a] 11% of bisaxial diacetyl derivative was isolated. [b] 9% of bisaxial diacetyl derivative was isolated. [c] 40% of bisaxial diacetyl derivative was isolated.

A possible mechanistic scenario for the reaction of diacetyl with aliphatics involves concerted insertion into the C–H bonds, single-electron transfer (SET) from the hydrocarbon, or hydrogen abstraction with triplet diacetyl. We first computed at different DFT and ab initio levels the bar-

riers for the concerted insertion that appears to be too high in energy ($\Delta H^{\ddagger}$ = 60–70 kcal mol^{-1}) to be relevant. The SET mechanism is also unlikely due to the high oxidation potential of saturated hydrocarbons (IP = 212 kcal mol^{-1} for adamantane[32]). Because diacetyl can readily be excited into high-lying states, the SET mechanism cannot be entirely excluded. A more realistic hydrogen radical abstraction mechanism with the triplet diacetyl diradical is supported by the high negative ρ^* values for the acetylation of adamantane derivatives.[33]

The selectivity of this reaction is unusually high for a radical substitution of the adamantane cage. We have shown previously that even with highly selective CI$_3$ radicals some 2-adamantane derivatives form as well.[34,35] Thermal metal-catalyzed adamantane C–H substitutions with diacetyl are also well documented but occur only in the presence of oxygen and with substantially lower selectivities.[36] Under these conditions, the peroxoacetyl radical MeC(O)OO· rather than the acetyl radical or diacetyl diradical were assumed to participate in the activation step.[36]

Currently, the regiospecificity for the tertiary C–H positional selectivities of the adamantane cage with diacetyl upon irradiation is difficult to explain within a traditional free-radical mechanism. The high apical selectivities for the photoacetylations of higher diamondoids require careful scrutiny.

In order to develop a proper kinetic model for the C–H photoacetylation reaction we first analyzed different species responsible for the activation step. Three entities may form in the course of photoacetylation with diacetyl: triplet diacetyl (from excitation and intersystem crossing of the singlet Ac$_2$ ground state), acetyl radical (from the photolysis of Ac$_2$), and peroxoacetyl radical (formed after trapping of the acetyl radical with oxygen that may be present in the reaction media in trace amounts). We first computed[37] the relative barriers for the hydrogen abstraction from the secondary and tertiary positions of adamantane with these three species (Figure 2).

It appears that the reaction with the acetyl radical is not particularly selective, because the barriers for hydrogen abstraction from the tertiary and secondary positions through TS1 and TS2, respectively, are the same within the computational errors [$\Delta\Delta H_{298}^{\ddagger}$ = 0.6 kcal mol^{-1}, B3LYP/6-31G(d)]. In contrast, the differences in the barriers for hydrogen abstraction with the triplet diacetyl diradical (TS3 and TS4), as well as with the peroxoacetyl radical (TS5 and

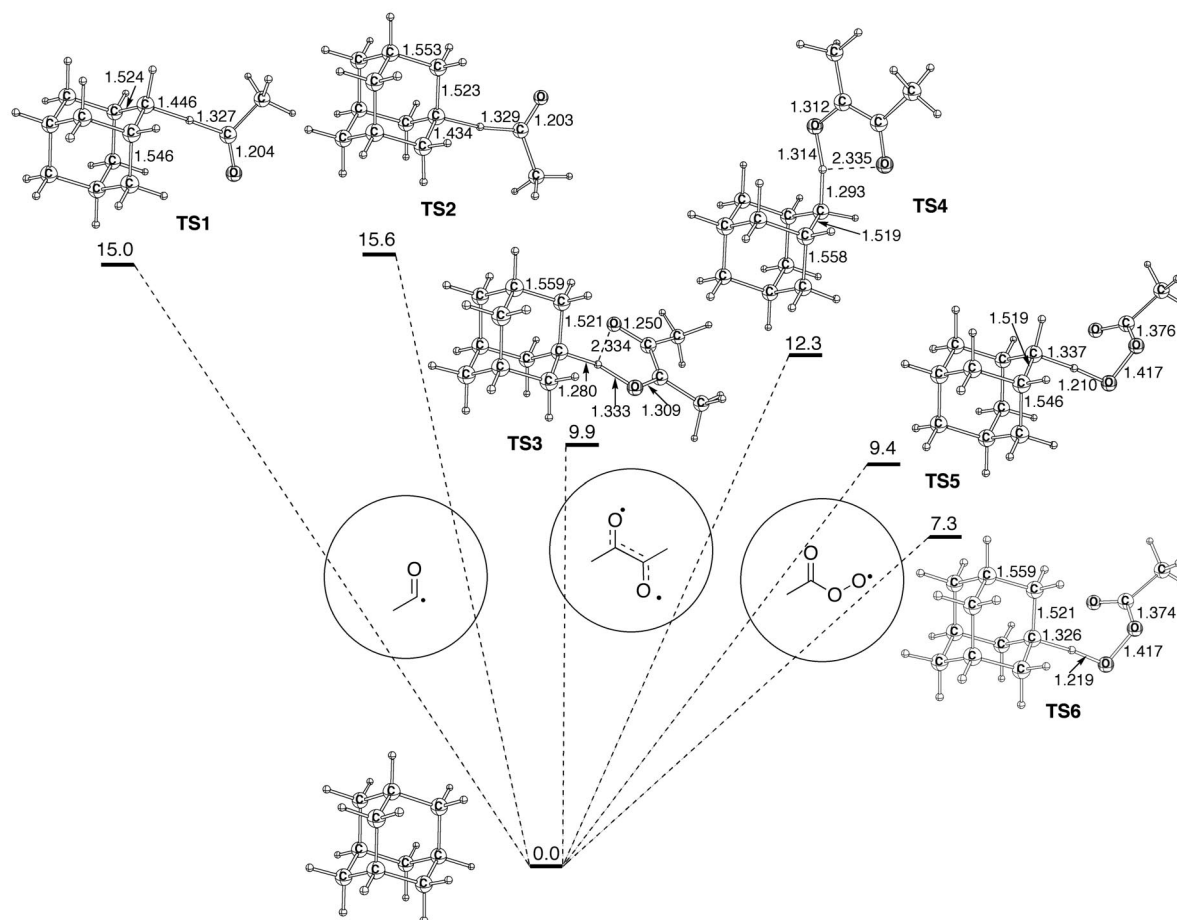Figure 2. Relative barriers (ΔH_{298}) for hydrogen abstraction from the tertiary and secondary positions of adamantane with the acetyl radical (TS1 and TS2), triplet diacetyl (TS3 and TS4), and the peroxoacetyl radical (TS5 and TS6) at B3LYP/6-31G(d).
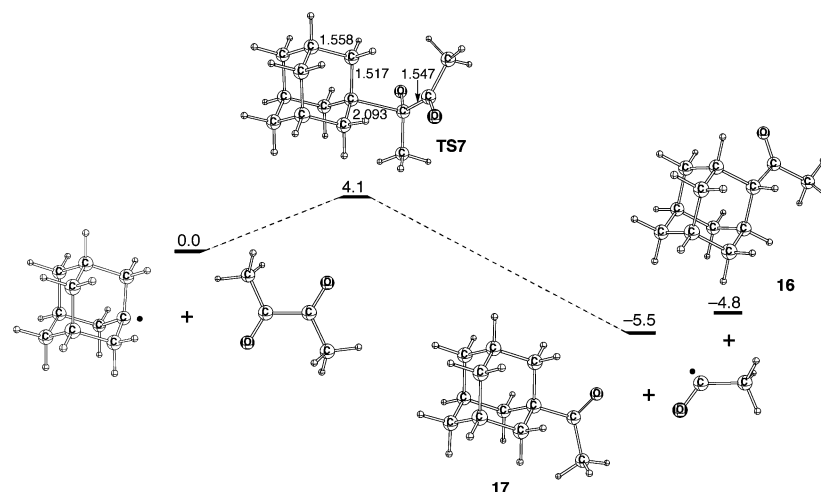
Figure 3. Barrier for trapping of the 1-adamantyl radical with diacetyl [B3LYP/6-31(d), ΔH_{298}] and the relative energies of 2-acetyl-(**16**) and 1-acetyladamantane (**17**).

TS6), are large enough ($\Delta\Delta H_{298}^{\ddagger}$ = 2.4 and 2.1 kcal mol^{-1}, respectively) to correspond to the high experimentally observed selectivities for the photoacetylation of adamantane. It is conceivable that the selectivity decrease previously observed in the photoacetylation of adamantane in the presence of oxygen[36] is not due to the suggested participation of peroxoacetyl radical but rather due to formation of other oxygen-centered radicals as found in the aerobic oxidations of adamantane.[21] We assume that both triplet diacetyl and the peroxoacetyl radical could be responsible for the high positional selectivities in the photoacetylation of adamantane in the presence of oxygen. However, under an inert atmosphere the participation of the peroxoacetyl radical is largely suppressed. The 1-adamantyl radical formed after hydrogen abstraction is effectively trapped with excess diacetyl: The barrier for this reaction is only 4.1 kcal mol^{-1} (Figure 3). However, the reverse reaction is endothermic by only 5.5 kcal mol^{-1} and is characterized by a moderate barrier ($\Delta H_{298}^{\ddagger}$ = 9.9 kcal mol^{-1}) and may compete with or even overrun hydrogen abstraction from adamantane with triplet diacetyl. The same is true for the equilibrium through hypothetically formed 2-acetyl adamantane (**16**). As 1-acetyl adamantane (**17**) is thermodynamically more stable than compound **16**, thermodynamic control that determines the selectivities of the photoacetylations cannot be excluded a priori.

To probe the nature of the rate-limiting step we measured the primary deuterium kinetic isotope effects (KIEs) for photoacetylation of adamantane versus 1,3,5,7-tetradeuterio adamantane in the presence of a large excess of diacetyl. The KIE values were calculated from the ratio of the monoacetylation products formed from the competition reaction between protio and deuterio adamantane on the basis of the mass-selective integration in the GC–MS. Large experimental KIEs would be taken as evidence for rate-limiting hydrogen abstraction and a kinetically controlled product ratio. The mechanistic model (Scheme 1) involves the formation of triplet diacetyl (*A*), slow hydrogen abstraction (*B*), and fast adamantyl radical trapping (*C*) with an excess amount of ground-state diacetyl.

As the reaction was carried out with a large excess of the reagent, that is, [AcAc]~[AcAc]$_0$, stationary conditions for triplet diacetyl (AcAc^T) are described by Equations (1) and (2).

$$\frac{d[\text{AcAc}^T]}{dt} = k_0[\text{AcAc}]_0 - k_{-0}[\text{AcAc}^T] - k_{1H}[\text{AcAc}^T][\text{Ad}_H] - k_{1D}[\text{AcAc}^T][\text{Ad}_D] = 0 \tag{1}$$

$$\frac{d[\text{Ad}^\bullet]}{dt} = k_1[\text{Ad}][\text{AcAc}^T] - k_2[\text{Ad}^\bullet][\text{AcAc}]_0 = 0 \tag{2}$$

The rate of the formation of the product, methyladamantyl ketone (AcAd, **17**), is determined from Equation (3).

$$\frac{d[\text{AcAd}]}{dt} = k_2[\text{Ad}^\bullet][\text{AcAc}]_0 = k_1[\text{Ad}][\text{AcAc}^T] \tag{3}$$

where

$$[\text{AcAc}^T] = \frac{k_0[\text{AcAc}]_0}{k_{-0} + k_{1H}[\text{Ad}_H] + k_{1D}[\text{Ad}_D]}$$

Because of the low quantum yield of the photoacetylation[33] only a small amount of photoexcited diacetyl (AcAc*) is consumed for formation of the products ($k_{-0} \gg k_{1H}, k_{1D}$). If we consider [AcAc^T] = k_x – constant, the reaction balance is determined with Equation (4).

$$\frac{[\text{AcAd}_H]}{[\text{AcAd}_D]} = \frac{[\text{Ad}_H]_0}{[\text{Ad}_D]_0}\frac{k_{1H}}{k_{1D}}\left(1 - \frac{(k_{1H} - k_{1D})k_x t}{2}\right) \tag{4}$$

From the experiment, the ratio of the products is described by Equation (5) with *r* = –0.982 and *n* = 8.
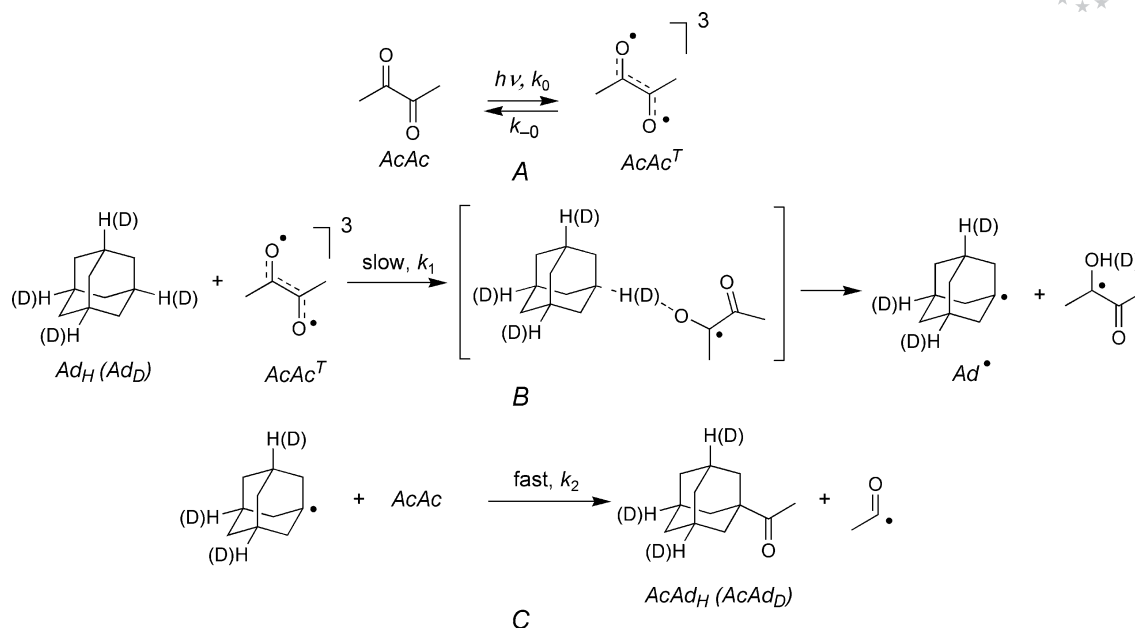
Scheme 1. Reactions considered in the experimental determination of the kinetic isotope effect of the photoacetylation of adamantane.

$$\frac{[\mathrm{AcAd_H}]}{[\mathrm{AcAd_D}]} = (4.00 \pm 0.075) - (0.275 \pm 0.022)t \tag{5}$$

Equation (5) leads to Equation (6) ($r = -0.967$, $n = 8$), which describes the ratio of concentrations of protio and deuterio adamantanes (Figure 4) in the course of the reaction:

$$\ln\frac{[\mathrm{Ad_H}]}{[\mathrm{Ad_D}]} = \ln\frac{[\mathrm{Ad_H}]_0}{[\mathrm{Ad_D}]_0} - (k_{1H} - k_{1D})k_x t = -(0.1337 \pm 0.012) - (0.0307 \pm 0.003)t \tag{6}$$

This gives the approximate ratio at $t = 0$, which differs from 1 as a result of high initial rates: $\dfrac{[\mathrm{Ad_H}]}{[\mathrm{Ad_D}]} = 0.874 \pm 0.010$. From the ratio of estimates [combining Equation (5) and (6) the experimental KIE value was obtained through Equation (7).

$$\frac{k_H}{k_D} = \frac{4.00 \pm 0.075}{0.874 \pm 0.010} = 4.58 \pm 0.13 \tag{7}$$

The relatively high experimental KIE value of 4.58 ± 0.13 is typical for adamantane reactions with radicals,[19,35] where the TSs are located roughly halfway along the reaction coordinate. The experimental KIEs were compared with the values computed by the Arrhenius and Bigeleisen[38] equations (Table 2) for *cis*-TS3 and as *trans* (higher in energy, not shown) conformeric transition structures. From these data we conclude that hydrogen abstraction is the rate-limiting step and that the selectivity of the photoacetylation reaction is determined kinetically.

We then applied this mechanistic model to higher diamondoids, where different tertiary positions may compete for the photoacetylation. The simplest model is diamantane
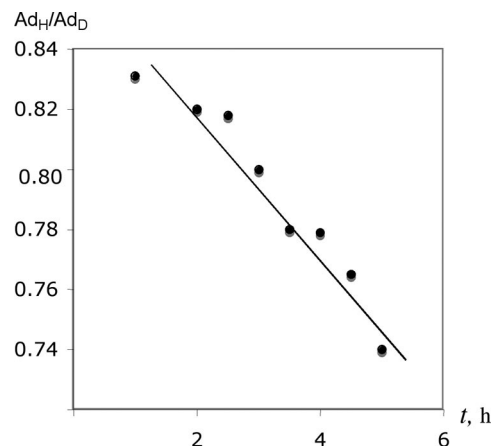
Figure 4. The dependence of the ratio of protio to deuterio adamantanes from the reaction time calculated through the ratio of the reaction products.

Table 2. The B3LYP/6-31+G(d) computed and experimental primary kinetic isotope effects for the reaction of adamantane with triplet diacetyl (TS3) and peroxoacetyl radical (TS6).

	A	ZPVE	KIE Arrhenius	KIE Bigeleisen	Expt.
cis-TS3	1.07	0.92	5.06	5.74	
trans-TS3	1.07	0.9	4.87	5.57	4.58 ± 0.13
TS6	1.22	0.8	4.71	5.16	

(**1**), for which four transition structures TS8–TS11 for the hydrogen abstraction with the triplet diacetyl diradical were located (Figure 5). The two low-lying *cis*-TS8 and TS10 are very close in energy; the energetic differences for conformeric TS9 and TS11 are even larger in favor of medial substitution. Qualitatively, the same picture emerges with other

Figure 5. The relative B3LYP/6-31G(d) energies [kcal mol^{-1}] of the transition structures for hydrogen abstraction from diamantane with the diacetyl triplet diradical in t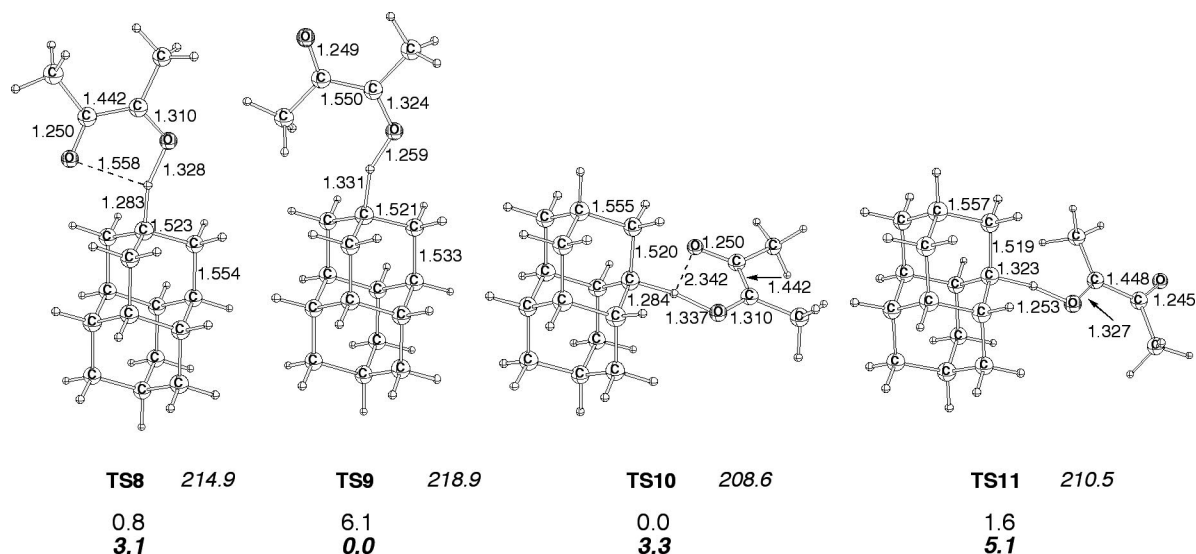he gas phase in CH$_2$Cl$_2$ (PCM, bold italics), and the polarizabilities of the transition structures (B^3, italics).

DFT functionals (BLYP, B3PW91) as well as with MP2 employing various basis sets. This is in marked contrast to the experimental observation that apical derivative **9** predominantly forms (Table 1). Thus, the gas-phase computations are not able to reproduce the experimental selectivities. We then examined the influence of the solvent utilizing polarized continuum model (PCM) computations in CH$_2$Cl$_2$ on the B3LYP/6-31G(d) optimized geometries. As a result of the much higher polarizabilities apical transition structures TS8 and TS9 are more stabilized in the condensed phase than medial TS10 and TS11, demonstrating that the solvent rather than steric or electronic factors determines the selectivity of the photoacetylation. However, exact matching of these theoretical data to the experiment is not completely valid, as medial substitution is statistically favored.

The higher diamondoid [1(2)3]tetramantane (**5**) appears to be a more relevant model, as it contains three pairs of tertiary hydrogen atoms in the 4,5,7-positions. We also employed the DFT method B3PW91, which is more trustworthy for large hydrocarbons than the B3LYP[39] method for energy evaluations.

As in the case of diamantane, the gas-phase computations place hydrogen abstraction TS13 from the medial 5-position below others (Figure 6).[40] However, the B3PW91/6-31G(d) PCM computations on the B3PW91/6-31G(d) gas-phase geometries favor hydrogen abstraction from the 7-position through TS12. This, again, is determined by the higher polarizabilities of the cage through the apical position (305.4 B^3 for TS12 vs. around 290 B^3 for TS13–TS15). This agrees well with the experimentally observed selectivity
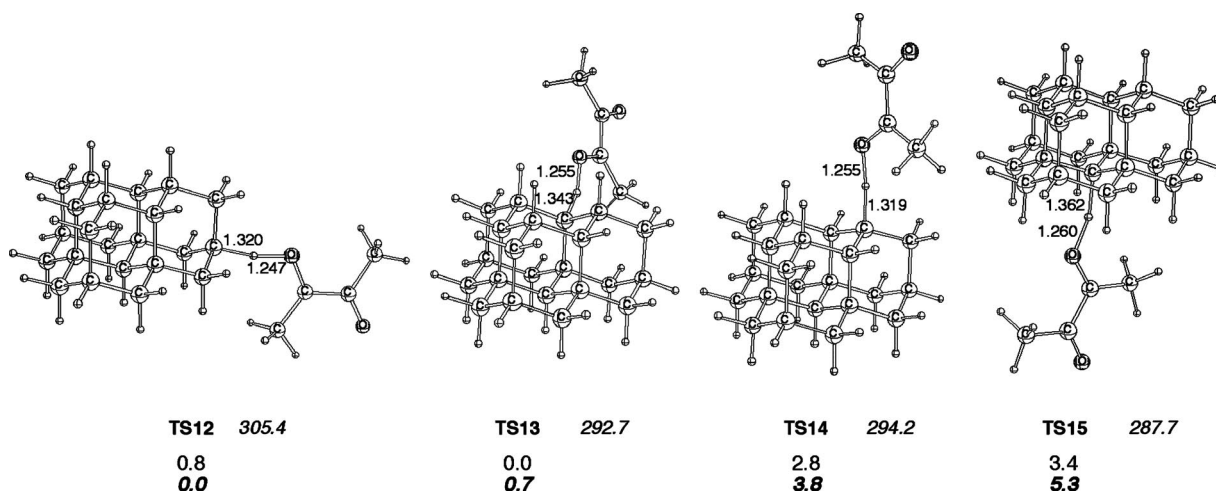

Figure 6. The relative B3PW91/6-31G(d) energies [kcal mol^{-1}] of the transition structures for hydrogen abstraction from [1(2)3]tetramantane with the diacetyl triplet diradical in the gas phase in CH$_2$Cl$_2$ (PCM, bold italics), and the polarizabilities of the transition structures (B^3, italics).

for the photoacetylation (Table 1). Thus, the solvent effects are needed to predict properly the selectivities in the reactions of triplet diacetyl for similarly reactive tertiary C–H bonds as those in [1(2)3]tetramantane (**5**). Steric effects play only a minor role. This conclusion is supported by the critical C–H and O–H bond lengths in the transition structures for hydrogen abstractions for which there is no simple correlation between the geometries and the relative energies of the TSs. Polar (charge transfer) effects, which often are responsible for the remarkable selectivities in reactions of alkanes in general and diamondoids in particular with electrophilic radicals such as PINO[21] or neutral metal–oxo reagents,[23] are insignificant in this case: The value of the NBO charge transfer from the hydrocarbon to diacetyl is 0.12 e in TS12 and is *larger* (0.19 e) in the highest-lying TS15. Thus, steric and solvent effects in the photoacetylations with diacetyl outweigh electron transfer effects that are the driving force for the medial cage substitutions with oxidizing electrophiles and electrophilic radicals.[1]

In the case of [1(2,3)4]pentamantane (**7**), owing to the presence of only two types of very different tertiary C–H bonds, even gas-phase computations correctly reflect the preferential substitution of the apical tertiary C–H bonds: Apical TS16 is 3.9 kcal mol^{-1} lower in energy than TS17, which describes the hydrogen abstraction from the medial position (Figure 7) and the PCM calculations enhance this difference even further in favor of TS16 as a result of its higher polarizability. Therefore, the apical products dominate in the experimental photooxidation of **7** with triplet

diacetyl (Figure 7). As a result of the high apical positional selectivity of this reaction, even the disubstitution of [1(2,3)4]pentamantane occurs selectively to give diketone **19**.

Conclusions

The photoacetylation of diamondoids with diacetyl displays unusually high tertiary C–H bond selectivities and gives apical acetyl diamondoids in high preparative yields. The limiting step of the reaction involves hydrogen abstraction with triplet diacetyl and is characterized by large kinetic isotope effects. The selectivities of the substitutions in solution are mostly determined by the higher polarizabilities of the cages in the apical direction. Steric effects play only a minor role, and in combination with solvation, outweigh charge transfer effects that usually favor medial substitution. Solvent effects must be included in the computations in order to predict the relative reactivities of diamondoids in photoacetylation reactions.

Experimental Section

General: NMR spectra were recorded with a Bruker Advance III spectrometer at 600 MHz (^{1}H) and 150 MHz (^{13}C); the chemical shifts are given in ppm relative to TMS. GC–MS analyses were performed with an HP5890 GC with an HP5971A mass-selective detector. 1,3,5,7-Tetradeuterioadamantane was prepared through the reduction of 1,3,5,7-tetrabromoadamantane as described previously.[41]

Photoacetylation of Adamantane and 1,3,5,7-Tetradeuterioadamantane: A solution of adamantane and 1,3,5,7-tetradeuterioadamantane in equimolecular quantities (1 mmol) and diacetyl (1 mL) in dichloromethane (5 mL) was irradiated in a quartz vessel with a high-pressure, 100-W mercury lamp with water cooling under an atmosphere of argon. Probes were taken and analyzed with a GC–MS column HP Ultra1 (50 m × 0.2 mm × 0.33 mm film: cross-linked methyl silicone) by mass-selective integration at m/z = 135 and 139 from the fragmentation of protio and deuterio acetyl adamantanes at the conversion of the starting material of less than 30%.

Photoacetylation of [1212]Pentamantane (4): A solution of **4** (130 mg, 0.38 mmol) and diacetyl (1.5 mL, 17.4 mmol) in CH$_2$Cl$_2$ (10 mL) was irradiated in a quartz vessel with a high-pressure, 150-W mercury lamp for 18 h under an atmosphere of argon. The mixture was concentrated under reduced pressure, and the residue was separated by column chromatography on silica gel (pentane/ether, 8:1) to give 75 mg (51%) of 13-acetyl[1212]pentamantane (**12**) as a colorless solid. M.p. 149–150 °C (hexane). ^{1}H NMR (600 MHz, CDCl$_3$, 25 °C): δ = 2.03 (s, 3 H, CH$_3$), 1.69–1.82 (m, 3 H), 1.70 (m, 4 H), 1.60–1.65 (m, 8 H), 1.35–1.18 (m, 14 H), 0.82 (m, 2 H) ppm. ^{13}C NMR (150 MHz, CDCl$_3$, 25 °C): δ = 214.1 (C), 52.5 (CH$_2$), 47.5 (CH), 47.4 (CH), 46.7 (C), 46.5 (CH), 44.9 (CH$_2$), 44.6 (CH$_2$), 44.3 (CH$_2$), 44.2 (CH$_2$), 38.7 (CH$_2$), 37.9 (CH$_2$), 37.8 (CH), 37.6 (CH), 37.0 (CH), 36.1 (CH), 34.1 (C), 33.1 (C), 28.9 (C), 27.7 (CH), 24.5 (CH$_3$) ppm. MS: m/z (%) = 386 (11), 343 (100), 239 (100), 193, 167, 141, 105, 91. HRMS: calcd. for C$_{28}$H$_{34}$O 386.2610; found 386.2596.

Photoacetylation of [1(2,3)4]Pentamantane (7): A solution of **7** (300 mg, 0.87 mmol) and diacetyl (6 mL, 70 mmol) in CH$_2$Cl$_2$

TS16 *342.7*   **TS17** *326.5*
0.0   3.9

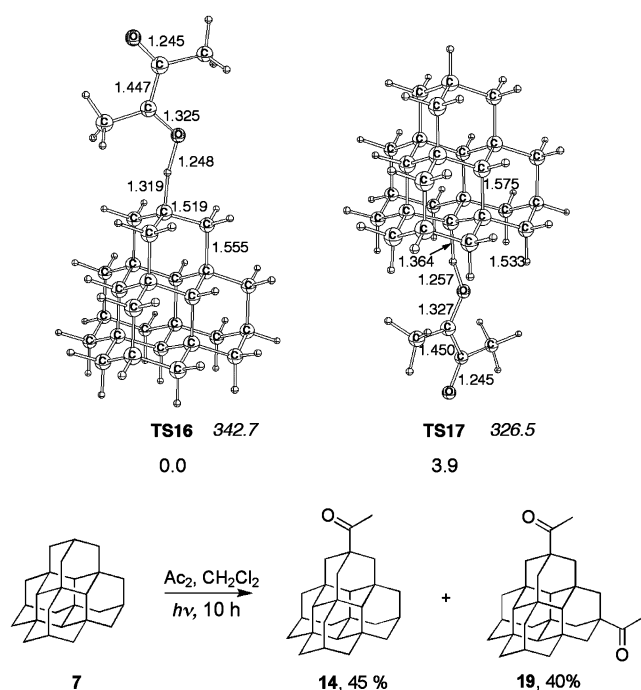Figure 7. The relative B3LYP/6-31G(d) energies [kcal mol^{-1}] of the transition structures for hydrogen abstraction with the diacetyl triplet diradical from the apical (TS16) and medial (TS17) positions of [1(2,3)4]pentamantane (**7**) in the gas phase, polarizabilities of the transition structures (B^3, italic), and the experimental results of the photoacetylation of **7** with diacetyl (yields are preparative).

(23 mL) was irradiated in a quartz vessel with a high-pressure, 150-W mercury lamp for 10 h under an atmosphere of argon. Column chromatography on silica gel (pentane/diethyl ether, 8:1) gave 167 mg (45%) of 7-acetyl[1(2,3)4]pentamantane (**14**) as a colorless solid. M.p. 130–132 °C (hexane). ^{1}H NMR (600 MHz, CDCl$_3$, 25 °C): δ = 2.02 (s, 3 H, CH$_3$), 1.84 (m, 3 H), 1.28 (m, 12 H), 1.25 (m, 12 H), 0.91 (s, 1 H), 0.85 (s, 3 H) ppm. ^{13}C NMR (150 MHz, CDCl$_3$, 25 °C): δ = 213.5 (C), 52.3 (CH), 51.8 (CH), 47.4 (C), 44.3 (CH$_2$), 43.7 (CH$_2$), 43.6 (CH$_2$), 32.2 (C); 31.7 (C), 27.3 (CH), 23.4 (CH$_3$) ppm. MS: m/z (%) = 386 (4), 343 (100), 239 (100), 193, 172, 143, 105, 91. HRMS: calcd. for C$_{28}$H$_{34}$O 386.2610; found 386.2656. C$_{28}$H$_{34}$O (386.56): calcd. C 87.00, H 8.87; found C 86.69, H 8.97. Elution with pentane/ethyl acetate (3:1) gave 149 mg (40%) of 7,11-diacetyl[1(2,3)4]pentamantane (**19**) as a colorless solid. M.p. 205–207 °C (hexane). ^{1}H NMR (600 MHz, CDCl$_3$, 25 °C): δ = 2.02 (s, 6 H, CH$_3$), 1.87 (m, 2 H), 1.28–1.35 (m, 24 H), 0.89 (s, 2 H), 0.81 (s, 2 H) ppm. ^{13}C NMR (150 MHz, CDCl$_3$, 25 °C): δ = 213.0 (C), 52.4 (CH), 51.8 (CH), 47.3 (C), 45.3 (CH$_2$), 45.0 (CH$_2$), 44.8 (CH$_2$), 44.4 (CH$_2$), 33.6 (C), 33.1 (C); 32.7 (C), 28.2 (CH), 24.4 (CH$_3$) ppm. HRMS: calcd. for C$_{30}$H$_{36}$O$_2$ 428.2715; found 428.2723. C$_{30}$H$_{36}$O$_2$ (428.61): calcd. C 84.07, H 8.47; found C 83.98, H 8.47.

Photoacetylation of [123]Tetramantane [($\pm$)-8]: A solution of ($\pm$)-**8** (100 mg, 0.34 mmol) and diacetyl (1.8 mL, 21.4 mmol) in CH$_2$Cl$_2$ (10 mL) was irradiated in a quartz vessel with a high-pressure, 150-W mercury lamp for 18 h under an atmosphere of argon, after which the mixture was concentrated under reduced pressure. The residue was separated by column chromatography on silica gel (pentane/diethyl ether, 8:1) to give 62 mg (56%) of 4-acetyl-[123]-tetramantane [($\pm$)-**15**] as a colorless solid. M.p. 108–110 °C (hexane). ^{1}H NMR (600 MHz, CDCl$_3$, 25 °C): δ = 2.32 (m, 1 H), 2.15 (m, 1 H), 2.08–1.95 (m, 2 H), 2.03 (s, 3 H, CH$_3$), 1.82–1.75 (m, 2 H), 1.68–1.55 (m, 12 H), 1.40–1.23 (m, 5 H), 1.15 (m, 2 H), 0.88 (m, 1 H), 0.82 (m, 1 H) ppm. ^{13}C NMR (150 MHz, CDCl$_3$, 25 °C): δ = 214.2 (C), 47.6 (CH), 47.3 (C), 47.2 (CH), 42.1 (CH), 42.0 (CH), 39.9 (CH$_2$), 39.1 (CH), 39.0 (CH$_2$), 38.9 (CH), 38.4 (CH$_2$), 38.0 (CH$_2$), 37.9 (CH), 37.8 (C), 37.7 (CH$_2$), 37.5 (CH), 37.4 (CH), 37.1 (CH), 37.0 (C), 36.8 (CH$_2$), 32.9 (CH$_2$), 32.0 (CH$_2$), 28.3 (CH), 24.5 (CH$_3$) ppm. MS: m/z (%) = 334 (6), 291 (100), 263 (<1), 249 (<1), 235 (<1), 221 (<1), 195 (1), 167 (2), (3), 141 (1), 129 (3). HRMS: calcd. for C$_{24}$H$_{30}$O: 334.2297; found 334.2305.

Supporting Information (see footnote on the first page of this article): x, y, z coordinates of the optimized structures; copies of the NMR spectra of new compounds.

Acknowledgments

[1] H. Schwertfeger, A. A. Fokin, P. R. Schreiner, *Angew. Chem. Int. Ed.* **2008**, *47*, 1022–1036.

[2] M. Baidakova, A. Vul', *J. Phys. D: Appl. Phys.* **2007**, *40*, 6300–6311.

[3] A. Krüger, *Angew. Chem. Int. Ed.* **2006**, *45*, 6426–6427.

[4] J. Ristein, F. Maier, M. Riedel, J. B. Cui, L. Ley, *Phys. Solid State* **2000**, *181*, 65–75.

[5] R. Kalish, *J. Phys. D: Appl. Phys.* **2007**, *40*, 6467–6478, and refs. therein.

[6] J. Ristein, *Diamond Relat. Mater.* **2000**, *9*, 1129–1137.

[7] O. A. Shenderova, V. V. Zhirnov, D. W. Brenner, *Crit. Rev. Solid State Mater. Sci.* **2002**, *27*, 227–356.

[8] V. V. Danilenko, *Phys. Solid State* **2004**, *46*, 595–599.

[9] A. Krüger, F. Kataoka, M. Ozawa, T. Fujino, Y. Suzuki, A. E. Aleksenskii, A. Y. Vul', E. Osawa, *Carbon* **2005**, *43*, 1722–1730.

[10] A. Krüger, Y. Liang, G. Jarre, J. Stegk, *J. Mater. Chem.* **2006**, *16*, 2322–2328.

[11] J. E. Dahl, S. G. Liu, R. M. K. Carlson, *Science* **2003**, *299*, 96–99.

[12] J. E. P. Dahl, J. M. Moldowan, T. M. Peakman, J. C. Clardy, E. Lobkovsky, M. M. Olmstead, P. W. May, T. J. Davis, J. W. Steeds, K. E. Peters, A. Pepper, A. Ekuan, R. M. K. Carlson, *Angew. Chem. Int. Ed.* **2003**, *42*, 2040–2044.

[13] A. A. Fokin, B. A. Tkachenko, P. A. Gunchenko, D. V. Gusev, P. R. Schreiner, *Chem. Eur. J.* **2005**, *11*, 7091–7101.

[14] A. A. Fokin, P. R. Schreiner, *Mol. Phys.* **2009**, *107*, 823–830.

[15] A. A. Fokin, P. R. Schreiner, N. A. Fokina, B. A. Tkachenko, H. Hausmann, M. Serafin, J. E. P. Dahl, S. Liu, R. M. K. Carlson, *J. Org. Chem.* **2006**, *71*, 8532–8540.

[16] P. R. Schreiner, N. A. Fokina, B. A. Tkachenko, H. Hausmann, M. Serafin, J. E. P. Dahl, S. Liu, R. M. K. Carlson, A. A. Fokin, *J. Org. Chem.* **2006**, *71*, 6709–6720.

[17] N. A. Fokina, B. A. Tkachenko, M. A. M. Serafin, J. E. P. Dahl, R. M. K. Carlson, A. A. Fokin, P. R. Schreiner, *Eur. J. Org. Chem.* **2007**, 4738–4745.

[18] A. A. Fokin, B. A. Tkachenko, O. I. Korshunov, P. A. Gunchenko, P. R. Schreiner, *J. Am. Chem. Soc.* **2001**, *123*, 11248–11252.

[19] A. A. Fokin, P. R. Schreiner, *Chem. Rev.* **2002**, *102*, 1551–1593.

[20] A. A. Fokin, T. E. Shubina, P. A. Gunchenko, S. D. Isaev, A. G. Yurchenko, P. R. Schreiner, *J. Am. Chem. Soc.* **2002**, *124*, 10718–10727.

[21] A. A. Fokin, P. R. Schreiner, *Adv. Synth. Catal.* **2003**, *345*, 1035–1052.

[22] P. R. Schreiner, A. A. Fokin, P. v. R. Schleyer, H. F. Schaefer III in *Fundamental World in Quantum Chemistry* (Ed.: E. Kryachko), Kluwer Academic, Dordrecht, **2003**, vol. II, pp. pp. 349–375.

[23] B. A. Tkachenko, T. E. Shubina, D. V. Gusev, P. A. Gunchenko, A. G. Yurchenko, P. R. Schreiner, A. A. Fokin, *Theoret. Exp. Chem.* **2003**, *39*, 90–95.

[24] P. R. Schreiner, A. A. Fokin, *Chem. Rec.* **2004**, *3*, 247–257.

[25] A. A. Fokin, B. A. Tkachenko, N. A. Fokina, H. Hausmann, M. Serafin, J. E. P. Dahl, R. M. K. Carlson, P. R. Schreiner, *Chem. Eur. J.* **2009**, *15*, 3851–3862.

[26] T. M. Willey, J. D. Fabbri, J. R. I. Lee, P. R. Schreiner, A. A. Fokin, B. A. Tkachenko, N. A. Fokina, J. E. P. Dahl, R. M. K. Carlson, A. L. Vance, W. Yang, L. J. Terminello, T. van Buuren, N. A. Melosh, *J. Am. Chem. Soc.* **2008**, *130*, 10536–10544.

[27] W. L. Yang, J. D. Fabbri, T. M. Willey, J. R. I. Lee, J. E. Dahl, R. M. K. Carlson, P. R. Schreiner, A. A. Fokin, B. A. Tkachenko, N. A. Fokina, W. Meevasana, N. Mannella, K. Tanaka, X. J. Zhou, T. van Buuren, M. A. Kelly, Z. Hussain, N. A. Melosh, Z.-X. Shen, *Science* **2007**, *316*, 1460–1462.

[28] W. A. Clay, Z. Liu, W. Yang, J. D. Fabbri, J. E. Dahl, R. M. K. Carlson, Y. Sun, P. R. Schreiner, A. A. Fokin, B. A. Tkachenko, N. A. Fokina, P. A. Pianetta, N. Melosh, Z.-X. Shen, *Nano Lett.* **2009**, *9*, 57–61.

[29] W. Zhang, B. Gao, J. Yang, Z. Wu, V. Carravetta, Y. Luo, *J. Chem. Phys.* **2009**, *130*, 054705.

[30] H. Schwertfeger, C. Würtele, M. Serafin, H. Hausmann, R. M. K. Carlson, I. M. Dahl, P. R. Schreiner, *J. Org. Chem.* **2008**, *73*, 7789–7792.

[31] I. Tabushi, S. Kojo, P. v. R. Schleyer, T. M. Gund, *J. Chem. Soc., Chem. Commun.* **1974**, 591.

[32] A. Bewick, C. J. Edwards, S. R. Jones, J. M. Mellor, *Tetrahedron Lett.* **1976**, *17*, 631–634.

[33] I. Tabushi, S. Kojo, K. Fukunishi, *J. Org. Chem.* **1978**, *43*, 2370–2374.

[34] P. R. Schreiner, O. Lauenstein, E. D. Butova, P. A. Gunchenko, I. V. Kolomitsin, A. Wittkopp, G. Feder, A. A. Fokin, *Chem. Eur. J.* **2001**, *7*, 4996–5003.

[35] O. Lauenstein, A. A. Fokin, P. R. Schreiner, *Org. Lett.* **2000**, *2*, 2201–2204.

[36] A. Kishi, S. Kato, S. Sakaguchi, M. Ishii, *Chem. Commun.* **1999**, 1421–1422.

[37] All computations were performed with the GAUSSIAN03 program suite (M. J. Frisch, G. W. Trucks, H. B. Schlegel, G. E. Scuseria, M. A. Robb, J. R. Cheeseman, J. A. Montgomery Jr., T. Vreven, K. N. Kudin, J. C. Burant, J. M. Millam, S. S. Iyengar, J. Tomasi, V. Barone, B. Mennucci, M. Cossi, G. Scalmani, N. Rega, G. A. Petersson, H. Nakatsuji, M. Hada, M. Ehara, K. Toyota, R. Fukuda, J. Hasegawa, M. Ishida, T. Nakajima, Y. Honda, O. Kitao, H. Nakai, M. Klene, X. Li, J. E. Knox, H. P. Hratchian, J. B. Cross, V. Bakken, C. Adamo, J. Jaramillo, R. Gomperts, R. E. Stratmann, O. Yazyev, A. J. Austin, R. Cammi, C. Pomelli, J. W. Ochterski, P. Y. Ayala, K. Morokuma, G. A. Voth, P. Salvador, J. J. Dannenberg, V. G. Zakrzewski, S. Dapprich, A. D. Daniels, M. C. Strain, O. Farkas, D. K. Malick, A. D. Rabuck, K. Raghavachari, J. B. Foresman, J. V. Ortiz, Q. Cui, A. G. Baboul, S. Clifford, J. Cioslowski, B. B. Stefanov, G. Liu, A. Liashenko, P. Piskorz, I. Komaromi, R. L. Martin, D. J. Fox, T. Keith, M. A. Al-Laham, C. Y. Peng, A. Nanayakkara, M. Challacombe, P. M. W. Gill, B. Johnson, W. Chen, M. W. Wong, C. Gonzalez, J. A. Pople, *Gaussian 03*, Revision D.02; Gaussian, Inc, Wallingford CT, 2004) utilizing analytical first and second energy derivatives, employing the three-parameter hybrid functional (B3LYP) with 6-31G(d)basis that usually performs well for radicals (see, for instance, D. J. Henry, C. J. Parkinson, L. Radom. L. Radom. *J. Phys. Chem. A* **2002**, *106*, 7927–7936). For the *x*, *y*, *z* coordinates and electronic energies of computed species, see the Supporting Information.

[38] J. Bigeleisen, M. Wolfsberg, *Adv. Chem. Phys.* **1958**, 15–76.

[39] P. R. Schreiner, A. A. Fokin, R. A. Pascal, A. de Meijere, *Org. Lett.* **2006**, *8*, 3635–3638.

[40] The relative reactivity of hydrocarbons in the radical reactions may correlate with the stability of the resulting radicals. However, our computations show that this is not the case for the photoacetylation reaction. The 7- and 5- [1(2)3]tetramantyl radicals are energetically identical from the gas-phase computations; the PCM calculations favor the 5-radical by ca. 8 kcal mol^{-1}.

[41] G. A. Olah, P. Ramaiah, C. B. Rao, G. Sandford, R. Golam, N. J. Trivedi, J. A. Olah, *J. Am. Chem. Soc.* **1993**, *115*, 7246–7249.